Vortex Nucleation in Superfluid ^{4}He

J. Steinhauer, K. Schwab, Yury Mukharsky, J. C. Davis, and Richard E. Packard
Physics Department, University of California, Berkeley, California 94720
(Received 15 February 1995)

We have determined the features of a universal energy barrier which mediates the thermal nucleation of quantized vortices. The barrier is deduced from measurements of the intrinsic phase slip critical velocity using both dc flow and single phase slip experiments. It appears that at a given temperature a single curve can predict the outcome of all intrinsic vortex nucleation experiments for flow through small apertures.

PACS numbers: 67.40.Vs, 47.15.Ki, 67.40.Hf

The effects of quantized vorticity in superfluid ^{4}He have been studied intensively for forty years [1]. However, until recently, the details of the vorticity creation process have remained elusive. This situation began to change when it was realized that the observed temperature dependence of the intrinsic critical velocity could be associated with a rate equation describing thermal activation of vortices over a velocity dependent energy barrier [2–4]. In this Letter we describe experiments which determine the nature of this energy barrier over a wide velocity regime in the temperature range $0.4 < T < 1.9$ K.

We study the flow of superfluid through a submicron aperture. Superfluid dissipation occurs when the flow through the aperture reaches a rather well-defined value, the critical velocity. At this velocity a small vortex element, nucleated near some local surface asperity or ridge in the aperture, grows in the ambient velocity field and ultimately crosses all the stream lines before annihilating at a distant boundary [5]. Such an event, which corresponds to a change in the quantum phase difference (across the aperture) of 2π, is known as a 2π phase slip and is a fundamental mechanism for superfluid energy dissipation [6,7].

The essence of our experiment is to measure, in two different ways, the rate, f, of phase slip events as a function of velocity and temperature. We extract the shape of a velocity- and temperature-dependent energy barrier for the creation of a vortex, $E^*(v,T)$, by relating our data to the Arrhenius law [8]:

$$f = e^{-E^*(v,T)/k_BT} \quad \text{where } E^* = E - k_BT \ln\Gamma . \qquad (1)$$

Here E is the kinetic energy barrier and the inverse time Γ (in Hz) involves the dynamics and configurations of the fluctuations. Previous experiments [9–11] have implicitly determined E^* and its velocity derivative for one velocity value for each temperature. We are able to determine E^* over a broad range of velocity. If $\ln\Gamma$ is assumed to vary weakly with velocity, then at fixed T, E^* differs from E by an additive constant. This permits comparison with energy calculations for specific models, such as a vortex half ring.

Our apparatus is essentially a superfluid-filled box surrounded by superfluid. One wall of the box contains a submicron-size hole. The wall facing the aperture contains a flexible metallized diaphragm which can be manipulated by the application of voltages to an adjacent parallel electrode. The diaphragm's position is monitored by a SQUID-based displacement transducer [12].

The potential energy of the stretched diaphragm couples to the flow kinetic energy in the aperture to create a well-defined normal mode for this superfluid oscillator [13]. In one type of experiment we drive the oscillator on resonance by applying an ac electrostatic drive. The oscillation amplitude builds until the velocity in the aperture reaches the critical velocity. At this point a phase slip occurs which removes a detectable amount of energy from the oscillator. By monitoring the diaphragm's position, the individual phase slips are detected [7,14].

In previous oscillator-type experiments [14,15], the individual phase slips are often seen to have magnitude $2\pi n$ where the integer $n \geq 1$. The $n > 1$ events complicate some of the analysis [e.g., see Eq. (5) below]. We believe that $n > 1$ events are caused by external, vibration-induced instabilities in the vortex as it crosses the aperture. To eliminate such artifacts from the data, we have developed an apparatus with very small internal dimensions. The idea is to make the interior dimensions so small that the lowest-lying acoustic plane wave mode (perpendicular to the aperture plane) is well above any ambient disturbance.

The "microcell" is produced on a single silicon wafer using microfabrication techniques [16]. The distance from the diaphragm to the opposite wall is 17 μm and the transverse dimensions of the interior space are 5 mm $\times$ 5 mm. The lowest-lying plane wave mode, perpendicular to the aperture, lies near 240 kHz. The Helmholtz resonant frequency of the cell is 40.7 Hz at low temperatures [17]. The aperture [18] itself is a slit with dimensions 0.38 μm $\times$ 1.25 μm placed in a 0.1 μm thick, smooth [19] silicon nitride wall.

As a demonstration of the acoustic noise immunity of this microcell, we report that in the oscillation experiments, *all* observed phase slips are of magnitude 2π, independent of the noise in the laboratory. This observation

 0031-9007/95/74(25)/5056(4)$06.00

gives us confidence that our data are untainted by multiple phase slip events or extrinsic activation processes.

Measurements of thousands of the individual phase slip velocities permit us to construct a histogram of these values. We integrate this histogram to find the probability, $P(v)$, of a vortex being created before a given velocity amplitude is reached. For these experiments we define the average critical velocity v_c^{ac} as the value of the velocity for which $P(v) = 1/2$. The statistical width of this distribution Δv_c is defined as the inverse slope of $P(v)$ evaluated at v_c^{ac}. This width is roughly $\sqrt{2\pi}$ larger than the standard deviation [20]. The inset (a) of Fig. 1 shows a typical example of $P(v)$ at one particular temperature. Figure 1 displays the temperature variation [21] of v_c^{ac}. In this figure we see that the critical velocity increases almost linearly with decreasing temperature. This behavior has been seen in several laboratories [3,9,22–24]. Inset (b) of Figure 1 shows the temperature variation of $\Delta v_c/v_{c0}$ where v_{c0} is the value obtained by extrapolating the linear portion of the curve v_c^{dc} vs T to $T = 0$. [See Fig. 1 and discussion below for the meaning of v_c^{dc}.]

Our goal is to extract from our data the parameter E^* as defined in Eq. (1). Since $\Delta v_c/v_c^{ac} \ll 1$, we may expand $E^*(v,T)$ to first order in a Taylor series about the value v_c^{ac}. We write Eq. (1) as

$$f = c_1 e^{c_2(v - v_c^{ac})} \quad \text{where } c_1 \equiv e^{-E^*(v_c^{ac},T)/k_BT}$$

$$\text{and} \quad c_2 \equiv -\frac{1}{k_BT}\frac{\partial E^*}{\partial v}\bigg|_{v_c^{ac}} . \tag{2}$$

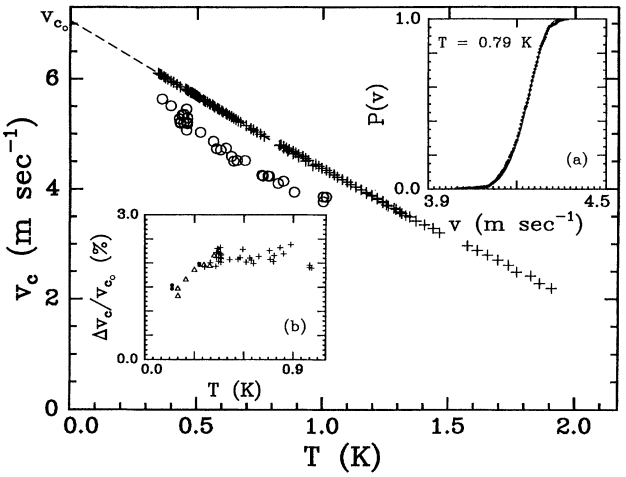

FIG. 1. The temperature variation of the average critical velocity. The open circles are v_c^{ac} and the plusses are v_c^{dc} measured at $\Delta P = 2$ Pa. Inset (a) shows the measured probability $P(v)$ for a phase slip to occur before the oscillating fluid velocity attains a value v. The black dots are the data. The solid line is from a simulation for a linear energy barrier. Inset (b) displays the width Δv_c of the distribution $P(v)$. The plusses are from the present experiment. The triangles are from Ref. [11], and the filled circles are from Ref. [10].

We write [25] $P(v)$ as a function of c_1 and c_2. We then find values of c_1 and c_2 that will produce the experimentally determined values of v_c^{ac} and Δv_c. These values of c_1 and c_2 are verified by numeric simulation. The solid curve in Fig. 1(a) shows the result of a typical simulation using the values of c_1 and c_2 appropriate for the data shown.

In Fig. 2, *which represent the fundamental results in this experiment,* the points designated with an asterisk and the associated line segment are the values of $E^*(v_c^{ac})$ and its derivative [26] $(\partial E^*/\partial v)|_{v_c^{ac}}$ obtained from the fit parameters c_1 and c_2, using the definitions in Eq. (2). The velocity determined by the diaphragm displacement transducer represents the velocity spatially averaged over the aperture. The relevant velocity near the nucleation site is presumed to be larger by a geometric factor which characterizes the microscopic surface structure near that site. For purposes of comparison between different apertures and experiments, we plot E^* as a function of the dimensionless velocity v/v_{c0}. If the only effect of microscopic surface structure is to determine a local velocity enhancement, then one expects that E^* would be a universal function of v/v_{c0}. However, if the vortex creation process involves vortex elements attached to surfaces, one might expect that $E^*(v/v_{c0})$ would vary from aperture to aperture.

It can be shown [10] that Δv_c can be written approximately in terms of the slope of the energy barrier $(\partial E^*/\partial v)|_{v_c^{ac}}$:

$$\Delta v_c = -\frac{2}{\ln 2} k_BT \left(\frac{\partial E^*}{\partial v}\bigg|_{v_c^{ac}}\right)^{-1} . \tag{3}$$

This expression does not account for the possibility of slipping in previous half cycles, which is required to determine E^*. Nevertheless, it gives values for the slope of the energy barrier which are within 1% of the values extracted from a more complete analysis [25]. Thus Eq. (3) is approximately valid, and Δv_c is inversely proportional to the slope of the energy barrier.

Figure 1(b) displays the temperature dependence of Δv_c. The plusses are from the present experiment. The closed circles and triangles are measurements for a nickel aperture, taken from Refs. [10] and [11], respectively. These latter data sets agree with our data in the overlapping temperature region. From Eq. (3) this implies that, within our signal to noise, the slope of the energy barriers is the same in all these experiments. It seems therefore that the precise microscopic structure of the aperture does not significantly affect the slope of the energy barrier. We note that now that we have determined the behavior of Δv_c at temperatures greater than 0.5 K, it is apparent that Δv_c does not simply vary linearly with temperature, a result expected when the energy barrier is linear in velocity, and both the attempt frequency and energy barrier are independent of temperature.

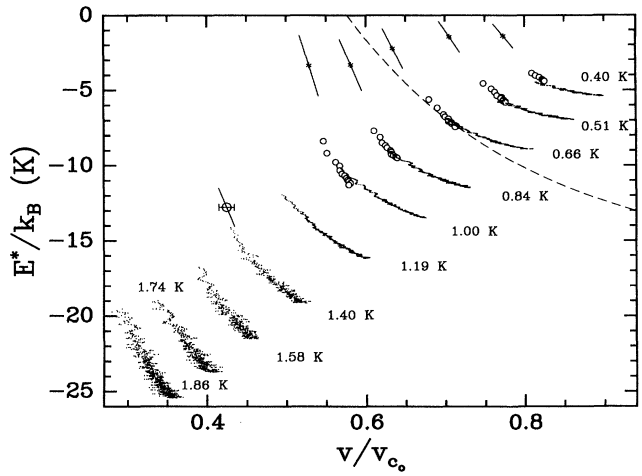

FIG. 2. The velocity dependence of E^* at various temperatures. The asterisks and associated straight line segments are derived from the present oscillation data. The dark continuous curve is from the present pressure-driven flow data. The circle data are from the experiment described in Ref. [24]. The open circle and its associated slope, lying near the 1.40 K data, are from Ref. [9].

To determine E^* at higher velocities we employ a quite different method. In this dc technique, we apply a voltage step between the diaphragm and the fixed adjacent electrode. This creates an abrupt pressure step which is relaxed by quasisteady flow through the aperture. The energy from the fluid pressure head is dissipated through a continuous sequence of individual phase slips, occurring at the Josephson-Anderson frequency

$$f_{\mathrm{JA}} = \frac{\Delta\mu}{\kappa}. \tag{4}$$

Here $\Delta\mu$ is the instantaneous chemical potential difference across the aperture, and κ is the circulation quantum. A value of $\rho\Delta\mu$ (where ρ is the liquid density) of 1 Pa corresponds to 69 kHz.

Using the displacement transducer, we record the diaphragm's instantaneous position $X(t)$ as the diaphragm moves toward its final position X_f. The pressure difference across the aperture is given by $\Delta P = k\{X_f - X(t)\}$, where k is the diaphragm's spring constant, 4×10^8 Pa/m. The average velocity in the aperture, derived by differentiating $X(t)$, is given by $\langle v\rangle = (\rho A_d/\rho_s a)\dot{X}$, where ρ_s is the superfluid density, A_d is the area of the diaphragm, and a is the aperture area (determined from electron microscopy).

f_{JA} is almost equivalent to the frequency f of Eq. (1) and $\rho\Delta\mu$ is almost the measured pressure difference $\Delta P(\langle v\rangle)$. Thus, from the measured $\Delta P(\langle v\rangle)$ and Eq. (1), $E^*(\langle v\rangle)$ can be extracted, and is shown by the continuous curves in Fig. 2. However, these curves contain small corrections (see discussion below) to determine f from f_{JA} and $\rho\Delta\mu$ from ΔP.

The chemical potential difference is given by $\Delta\mu = \Delta P/\rho - s\Delta T$, where s is the specific entropy and ΔT is the small temperature difference across the aperture which is induced by the thermomechanical effect. We measure $s\Delta T$ (which is at most 6% of the maximum ΔP in a transient) by a method identical to Ref. [27].

The actual velocity in the aperture must consist of a rapid sawtooth pattern as the fluid velocity continually jumps between a value near the average critical velocity and a lower value, after energy is removed by an individual phase slip. The average velocity in the aperture is related to the critical velocity for phase slips by [28]

$$v_c^{\mathrm{dc}} = \langle v\rangle + \frac{n\kappa}{2\ell}, \tag{5}$$

where ℓ is the effective hydrodynamic length of the aperture and n is the integer size of the phase slip in units of 2π. We use the notation v_c^{dc} to designate the average critical velocity for phase slips as measured in a dc flow experiment. The second term on the right-hand side of Eq. (5) represents a few percent correction for $n = 1$ which, as stated above, is the only size of phase slip observed in this apparatus.

The frequency of phase slips, Eq. (1), is almost the Josephson-Anderson frequency Eq. (4), the difference lying in the fact that the pressure-driven flow is not at constant velocity. The average velocity is less than the critical velocity [Eq. (5)] so f_{JA} is less than f. One can correct for this fact using an analysis that integrates the probability during the acceleration process between slips [28]. The final result amounts to a correction factor, $\gamma < 1$, such that $f_{\mathrm{JA}} = \gamma f$ [25]. One then obtains, from Eq. (1), $E^* = -kT\ln(\Delta\mu/\gamma\kappa)$. If this correction were not made, the continuous curves in Fig. 2 would be at most 0.8 K higher.

In Fig. 2 the dark curves are derived from flow transients in the microcell. One can make a rough estimate of the minimum value of E^* from the trend in E^* at large velocity. Assuming that Γ is independent of v, this value

is $-k_B T \ln\Gamma$. The data in Fig. 2 therefore suggest Γ is approximately e^{16} Hz at 1 K.

The circle data points on the curves are derived from flow transient data obtained with a different aperture (0.2 μm $\times$ 0.2 μm) in a completely different apparatus [24], yet this data set is consistent with the data from the microcell.

To further test the universality of the E^* curve, we have evaluated E^* and its derivative from the published data of Ref. [9], which reports critical velocities for a 9 μm nickel aperture. These data are represented by the line and circle at 1.4 K. Since those data only extend down to 1.3 K, it is difficult to determine v_{c0}. The horizontal line through the circle indicates this uncertainty [25].

The striking fact is that the data of Ref. [9] are fully consistent with our curves of E^*, as are the circle data points discussed above. Remember that Fig. 1(b) also gives this consistent result. The apparently universal form of $E^*(v/v_{c0})$ would suggest an underlying mechanism which is, except for a simple velocity enhancement, independent of microscopic surface structure. As stated above, if the vortex creation process involves vortex elements attached to surfaces [5], the exact microscopic surface structure should change the form of E^* for different specimens.

As a comparison to a specific model, we fit a half vortex-ring model [11,27] to E^* at 0.66 K. We assume that $\ln\Gamma$ is independent of velocity. Regardless of the core size, the model gives a curve whose curvature is much too small to fit the data.

We conclude by emphasizing that, by Eq. (1), the energy E^* contains all the details of the thermal fluctuations. Therefore Fig. 2 contains all the information to make a consistent set of predictions for the behavior of phase slippage phenomena involving either individual phase slips, as seen in oscillator experiments, or high frequency steady-state phase slips occurring at frequencies as great as 700 kHz. The remaining challenge now is to find the microscopic theory leading to the energy E and the factor Γ.

We acknowledge many helpful discussions with Stefano Vitale and Scott Backhaus. George Hess provided a preprint of Ref. [27] which helped us understand the $s\Delta T$ corrections. Ajay Amar contributed to an early version of this experiment and provided the aperture used in Ref. [24]. This research was supported by grants from the Office of Naval Research and the National Science Foundation.

[1] A recent review is given by R. J. Donnelly, *Quantized Vortices in HeII* (Cambridge University Press, New York, 1991).

[2] W. F. Vinen, in *Liquid Helium,* edited by G. Careri (Academic Press, New York, 1963), p. 336.

[3] E. Varoquaux, M. W. Meisel, and O. Avenel, Phys. Rev. Lett. **57**, 2291 (1986).

[4] P. C. Hendry *et al.,* Phys. Rev. Lett. **60**, 604 (1988).

[5] S. Burkhart, M. Bernard, O. Avenel, and E. Varoquaux, Phys. Rev. Lett. **72**, 380 (1994).

[6] P. W. Anderson, Rev. Mod. Phys. **38**, 298 (1966).

[7] O. Avenel and E. Varoquaux, Phys. Rev. Lett. **55**, 2704 (1985).

[8] Reaction rate theory is reviewed in P. Hänggi, P. Talkner, and M. Borkovec, Rev. Mod. Phys. **62**, 251 (1990).

[9] George B. Hess, Phys. Rev. Lett. **27**, 977 (1971).

[10] E. Varoquaux, W. Zimmermann, Jr., and O. Avenel, in *Excitations in Two and Three Dimensional Quantum Fluids,* edited by A. F. G. Wyatt and H. J. Lauter (Plenum, New York, 1992).

[11] O. Avenel, G. G. Ihas, and E. Varoquaux, J. Low Temp. Phys. **93**, 1031 (1993).

[12] H. J. Paik, J. Appl. Phys. **47**, 1168 (1976); our SQUID based displacement detector has an rms resolution of 1.6×10^{-13} m Hz$^{-1/2}$.

[13] B. P. Beecken and W. Zimmermann, Jr., Phys. Rev. B **35**, 74 (1987).

[14] A. Amar, Y. Sasaki, R. Lozes, J. C. Davis, and R. E. Packard, Phys. Rev. Lett. **68**, 2624 (1992).

[15] O. Avenel, M. Bernard, S. Burkhart, and E. Varoquaux, Physica (Amsterdam) B (to be published).

[16] K. Schwab (to be published).

[17] The thermomechanical effect slightly increases the frequency above 1 K. At 1.4 K, where $Q = 6$, the natural frequency is 44.1 Hz.

[18] A. Amar, R. L. Lozes, Y. Sasaki, J. C. Davis, and R. E. Packard, J. Vac. Sci. Technol. B **11**, 259 (1993).

[19] The surface of the aperture appears smooth in an electromicrograph picture resolving 40 nm.

[20] We use these definitions to permit direct comparison with Ref. [10].

[21] Thermometry was based on a Matsushita resistance thermometer calibrated against a Ge resistance thermometer.

[22] B. P. Beecken and W. Zimmermann, Jr., Phys. Rev. B **35**, 1630 (1987).

[23] M. Bonaldi, S. Vitale, and M. Cerdonio, Phys. Rev. B **42**, 9865 (1990).

[24] J. C. Davis, J. Steinhauer, K. Schwab, Yu. M. Mukharsky, A. Amar, Y. Sasaki, and R. E. Packard, Phys. Rev. Lett. **69**, 323 (1992).Phys. Rev. Lett. **69**, 323 (1992).

[25] J. Steinhauer *et al.* (to be published); Ph.D. thesis, University of California, Los Angeles, CA, 1995.

[26] In the notation of Ref. [10], $(\partial E^*/\partial v)|_{v_c^{ac}} = -E_0/v_{c0}$.

[27] G. M. Shifflett and G. B. Hess, J. Low Temp. Phys. (to be published).

[28] R. E. Packard and S. Vitale, Phys. Rev. B **45**, 2512 (1992).